Check for updates

Detection of mitotic cells in breast cancer histopathological images using deep versus handcrafted features

I. Onur Sigirci[1] · Abdulkadir Albayrak[2] · Gokhan Bilgin[3] (iD)

Abstract

One of the most important processes in the diagnosis of breast cancer, which is the leading mortality rate in women, is the detection of the mitosis stage at the cellular level. In literature, many studies have been proposed on the computer-aided diagnosis (CAD) system for detecting mitotic cells in breast cancer histopathological images. In this study, comparative evaluation of conventional and deep learning based feature extraction methods for automatic detection of mitosis in histopathological images are focused. While various handcrafted features are extracted with textural/spatial, statistical and shape-based methods in conventional approach, the convolutional neural network structure proposed on the deep learning approach aims to create an architecture that extracts the features of small cellular structures such as mitotic cells. Mitosis detection/counting is an important process that helps us assess how aggressive or malignant the cancer's spread is. In the proposed study, approximately 180,000 non-mitotic and 748 mitotic cells are extracted for the evaluations. It is obvious that the classification stage cannot be performed properly due to the imbalanced numbers of mitotic and non-mitotic cells extracted from histopathological images. Hence, the random under-sampling boosting (RUSBoost) method is exploited to overcome this problem. The proposed framework is tested on mitosis detection in breast cancer histopathological images dataset provided from the International Conference on Pattern Recognition (ICPR) 2014 contest. In the results obtained with the deep learning approach, 79.42% recall, 96.78% precision and 86.97% F-measure values are achieved more successfully than handcrafted methods. A client/server-based framework has also been developed as a secondary decision support system for use by pathologists in hospitals. Thus, it is aimed that pathologists will be able to detect mitotic cells in various histopathological images more easily through necessary interfaces.

Keywords Digital histopathology · Mitosis detection · Deep learning · Convolutional neural networks · Image spatial statistics · Imbalanced data

✉ Gokhan Bilgin
gbilgin@yildiz.edu.tr

Extended author information available on the last page of the article

1 Introduction

Breast cancer is the most common cancer type among women according to statistics released by World Health Organization (WHO). It is also the second leading cancer type causing mortality in women [45]. Cancer awareness, fertility and breastfeeding are some of the responsible factors for breast cancer [9]. For example, the incidence of cancer in developed countries is higher than in developing countries; because fertility and breastfeeding are less common in developed countries than developing countries. In contrast, women in developed countries are more aware of cancer risk than women in developing countries. It is clear that awareness is also an advantage for early detection of breast cancer [13, 38]. In conclusion, early detection of breast cancer plays an important role in the treatment and recovery stages.

Clinical and pathological diagnostic approaches are the most common methods used by experts to diagnose breast cancer. Generally, the presence of tumor structures is determined by examining the tissue samples taken from the patients by pathological methods. In this study, presence of mitosis, which is a sub-category of tumor detection, is investigated in histopathological imaging. In these images, tissue samples used in pathological operations are examined according on predefined criteria determined by the cancer grading system [1, 15]. These fundamental criteria are defined according to the following characteristics:

- Nuclear Pleomorphism
- Tubular Formation
- Mitosis detection

This study focuses on the detection of mitosis using deep versus handcrafted features in high resolution breast cancer histopathological images. The detection framework identified in the study aims to assist pathologists in examining mitotic figures in images. Because the process of identifying mitotic figures is a very difficult and time-consuming task for pathologists. Although images are taken from high-resolution scanners, it is challenging to make an exact decision as to whether the suspect cell is mitotic or not. Moreover, miscalculation of the number of mitotic cells in certain regions may lead to misdiagnosis. Therefore, a second reader/diagnostic aid system, which is good at visualization and achieves high accuracy, is essential to assist experts in pathology.

In recent years, many studies have been done to develop reliable, robust and automated computer-aided diagnosis (CAD) systems for mitosis detection. The general initial phase in previous studies is the separation of nuclei/foreground objects from background objects (stroma, blood cells, cytoplasm and adipose tissues, etc.). To ensure a better separation of cellular and non-cellular structures, the histopathological image should not contain too much noise that could distort the foreground and background objects.

Filtering and thresholding are common methods for noise reduction and there are many studies in the literature on noise reduction in high resolution histopathological images [24, 31, 44]. In threshold-based approaches, the boundary of cellular structures is better preserved than filtering-based methods. In this way, the discriminative features can be extracted without damaging the subsequent stages, detection, segmentation or classification. As a result, it can be said that preprocessing steps are very important for feature extraction and image segmentation steps from the perspective of pattern recognition and machine learning.

After noise reduction stage, the segmentation process is performed before the feature extraction phase which has a crucial importance for an accurate classification. In the literature, there are many studies that use segmentation for detection of cellular structures [17, 21]. For instance, in [19], a cell nuclei detection and segmentation algorithm is proposed for neuroblastoma by using the morphological top-hat by reconstruction method. In [20], histopathological tissue segmentation is proposed using fuzzy spatial clustering, vector-based multiphase level set active contours and nuclei detection using an iterative kernel voting scheme. As a post-processing phase, unnecessary or improperly classified non-cellular structures may be segmented as cellular fragments in final segmentation map. To eliminate these parts, mathematical morphological operations can be applied to obtain a better segmented image. In [12], morphological mathematical opening and closing operations are performed to fill up holes after segmentation. In [7], mathematical dilation and erosion operations are performed to improve the quality of the segmentation results.

Following to segmentation stage, feature extraction phase and classification of cellular structures are performed after identifying the cellular structures obtained in segmentation phase. Feature extraction algorithms used in the image processing differ depending on the properties of the image such as texture and shape. There are several published studies on feature extraction algorithms that focus on texture or shape information in histopathological images [14, 37, 50, 51]. Because such algorithms focus on one aspect of the image, they may fail with different types of images. As an example of a problem-specific solution, an algorithm that extracts shape-based features may not be able to extract different features in the image that contain texture information. Recently, deep learning algorithms that can be adapted to all kinds of image features and characteristics have been developed. Discriminatory features can be extracted from raw image data using deep learning-based algorithms as well as conventional extraction methods. However, deep learning-based algorithms give much more successful results in segmentation and classification problems where conventional methods are insufficient [2, 4, 5, 23, 36, 40, 52]. In biomedical image analysis, deep learning-based algorithms are also successfully used in the evaluation of histopathological, computed tomography (CT), magnetic resonance (MR) and ultrasound (US) imaging [6, 30, 32, 47, 48]. Convolutional neural networks, a fundamental architecture in deep learning, have also been proposed for the detection of mitosis in breast cancer histopathological images [8]. In [46], a hierarchical learning workflow is recommended for automated mitosis detection in breast cancer. In that study, an initial training set is used to learn the segmentation of candidate cells and these candidate cells are classified as mitotic or non-mitotic using object shape and tissue properties.

As stated in [27, 28], many mitosis detection systems may fail to classify mitotic and non-mitotic cells due to the imbalanced data. In [26], a training set consisting of a balanced mix of mitotic and non-mitotic cells is selected to prevent degradation of classification accuracy. In [25], data consistency is achieved by using the synthetic minority over sampling technique (SMOTE) by increasing the number of mitotic samples in the training dataset.

In this study, we aim to compare the performance of the handcrafted feature extraction algorithms and deep learning based feature extraction method. Hence, textural, shape and statistical based conventional handcrafted methods are employed besides deep learning based method. In the deep learning-based approach proposed specifically for this study, an appropriate architecture was created by focusing on the detection of small cellular structures such as mitotic cells. With the framework created in the study, feature extraction methods with different qualities based on both conventional and deep learning are presented as input

to the specified steps. In the first step, a 9×9 median filter is applied to the images to reduce the random noise and to preserve the boundary of cells for an efficient segmentation. Median filter size was selected empirically after different trials made specifically for histopathological images. Then, the k-means clustering algorithm is basically applied to segment cellular and non-cellular structures in an image. After segmentation step, morphological operations are performed to eliminate the irrelevant parts of cellular structures that actually belong to background structures in the images. Both mitotic and non-mitotic cellular structures are surrounded by a window to create image patches (as a region of interest) from where features are extracted. Afterwards, conventional handcrafted and deep learning-based feature extraction methods to be used on these patches are employed for comparisons. To improve the data consistence of the dataset, a robust class imbalance handling algorithm namely random under-sampling boosting (RUSBoost) which is an improved version of SMOTE technique is utilized.

The paper is organized as follows. Section 2 describes conventional handcrafted and deep learning based approaches for feature extraction. The proposed computer aided diagnosis framework is explained in detail In Section 3 and the findings of experimental studies are described in Section 4. Application software created to facilitate the workload of pathologists working on histopathology is introduced in Section 5. In the final sections of the paper, conclusions and discussions parts are presented in Section 6 and in Section 7 respectively.

2 Methods

2.1 Conventional handcrafted feature extraction algorithms

The detection of a particular object can be very challenging in many image processing and pattern recognition applications, depending on the discriminative features extracted from the object. Applying shape-based and texture-based algorithms are common way to extract certain distinctive features. Shape-based algorithms can help detect objects if discriminative features relate to shape information. On the other hand, texture-based algorithms are related to spatial relationships of pixels in a particular image. However, textural features are more reliable than the shape features in histopathological images in mitosis detection. Some samples about mitotic and non-mitotic cells are given in Fig. 1 for visual evaluation of shape and texture differences.

Remarkable and important techniques found in the biomedical literature (ie, completed local binary patterns, histogram of directed gradients, gray level coexistence matrices, local phase quantization and segmentation-based fractal tissue analysis) and some specific local statistical features are presented in comparison with the proposed method. This section aims to introduce the methods used for comparison.

2.1.1 Completed local binary patterns (CLBP)

Local binary pattern (LBP) is a texture descriptor algorithm that examines the adjacency of neighbor pixels and finds the patterns by using produced histogram [33]. The calculation of the histogram for a pixel is defined as:

$$
\begin{aligned}
LBP_{P,D} &= \sum_{p=0}^{P-1} t\left(g_p - g_c\right) 2^p \\
t(x) &= \begin{cases} 1 & x \geq 0 \\ 0 & x < 0 \end{cases}
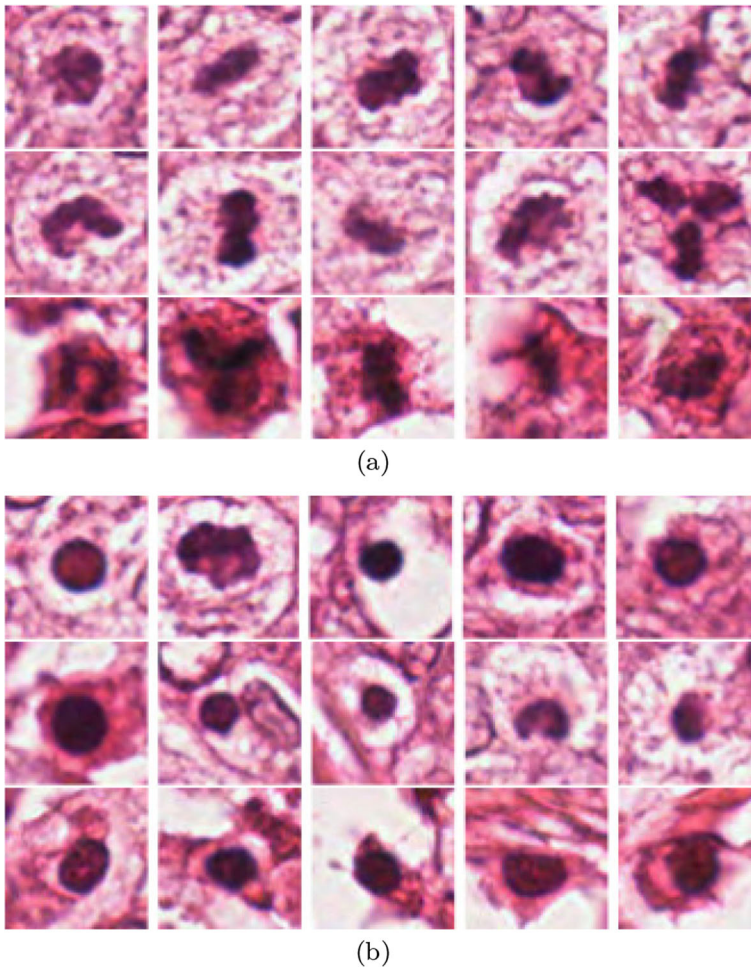\end{aligned} \tag{1}
$$

(a)

(b)

Fig. 1 Samples of **a** mitotic and **b** non-mitotic cells

where g_c represents the gray-scale value of the center pixel and g_p represents the gray-scale values of adjacent pixels. The value of P is the total neighbor pixels and D is the distance between the center pixel and the adjacent pixels. In this study, the R value is accepted as one. So, there are 8 neighbors of the related center pixel. The threshold function of t controls whether the value of the neighbor pixel is less than the value of the center pixel or not. Then, a histogram is obtained according to the LBP results. The formula of the histogram for an input image with $M \times N$ dimension is created as follows (The value of K shows the largest value that can be obtained in LBP, where $k \in [0, K]$):

$$H(k) = \sum_{i=1}^{M} \sum_{j=1}^{N} f\left(LBP_{P,D}(i,j), k\right)$$
$$f(x, y) = \begin{cases} 1 & \text{if } x = y \\ 0 & \text{Otherwise} \end{cases} \tag{2}$$
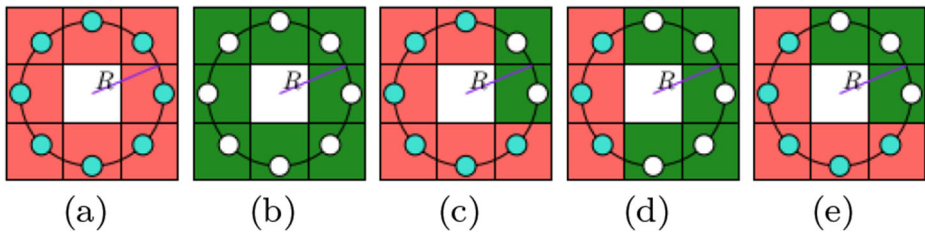
Fig. 2 Pixels which have value greater than or equal to the threshold is represented with filled circle and pink background, the other pixels which have smaller value are represented with empty circle and green background. Each of figure represented above show the possible situation when 0-transition or 2-transition **a** Dot **b** Dot/Line **c** Line **d** Edge **e** Corner

The number of $(0 - to - 1)$ and $(1 - to - 0)$ transition (U) is described as:

$$U(LBP_{P,D}) = |t(g_{P-1} - g_c) - t(g_0 - g_c)| + \sum_{P-1}^{p=1} |t(g_p - g_c) - t(g_{p-1} - g_c)| \quad (3)$$

The LBP algorithm is performed in a circular structure in the computation of U. Two transitions $(1-to-0$ or $0-to-1)$ or no transition code are used for the binary representation of uniformly distributed LBP pattern $(U \leq 2)$. This is shown by $LBP_{P,D}^{u2}$ notation. Sample transitions are represented in Fig. 2 according to the notation. In this study, due to the definition of P value as eight, the number of values that provides $U \leq 2$ becomes 58. The number of transitions more than 2 are assumed to be noise and they are added to the index of 59 in the histogram.

The distance of each neighbor pixel to the center has also a crucial role in completed local binary pattern (CLBP) as well as obtaining the histogram by LBP. The similarity of the center pixel to the neighbor pixels is also determined by the computed distance. Figure 3 represents an example of computed value from a pixel by using CLBP.

Similar to LBP, a 1×59 vector of values is created in CLBP when the value of P is 8 and the value of R is 1. A 1×59 vector also created to represents the distance of neighbor pixels to the center pixels. Totally, there is a size of 1×118 feature vector for each image patch to be used in classification step.
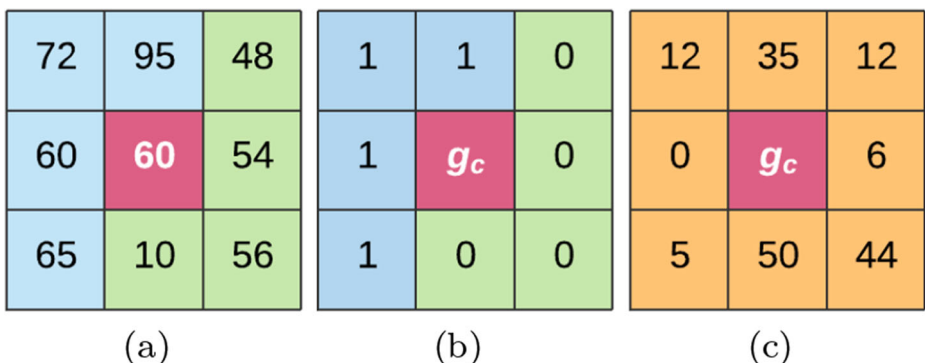

Fig. 3 **a** An example of 3×3 pixel area, **b** LBP code, **c** absolute values of distances to the central pixel

2.1.2 Histogram of oriented gradients (HOG)

Shape information is one of the main significant feature between mitotic and non-mitotic cells. In general, mitotic cells have a convex or concave shape while non-mitotic cells have an elliptic shape. HOG is shape-based feature extraction algorithm proposed by Dalal and Triggs for pedestrian detection [11]. The first research about HOG was on human detection in images but it is used for the purpose of object detection in many image processing and computer vision studies [16, 42]. HOG basically takes into account the gradients of edges to obtain discriminative features. An edge detection algorithm (such as Sobel, Canny) is implemented in vertical and horizontal directions of an image before calculating the gradients for all pixels. The vertical and horizontal edge detection formula can be shown as:

$$I_x = I \times S_x, \quad I_y = I \times S_y \tag{4}$$

where S_x and S_y represent the gradient masks that are applied vertically and horizontally to image. By using I_x and I_y, the gradients and their magnitude values are calculated as:

$$|G| = \sqrt{I_x^2 + I_y^2} \tag{5}$$

where G is the gradients calculated for each pixel and θ is the magnitude of that gradient.

$$\Theta = \arctan(G) \tag{6}$$

2.1.3 Gray level co-occurrence matrices (GLCM)

GLCM is a texture descriptor algorithm that is proposed by Robert Haralick [22]. This algorithm focuses on spatial relationship of neighbor pixels with each other. It basically calculates the adjacency of a pixel i to another pixel j in a given image. An example input image patch is shown in Fig. 4a for the computation of gray level co-occurrence matrix. Figure 4b represents the adjacency matrix of the given input image represented in Fig. 4a. The value written to the first row and first column of Fig. 4b represents in the number of 0 followed by 0 in the given input image. Since there is only one 0 followed by 0, the value
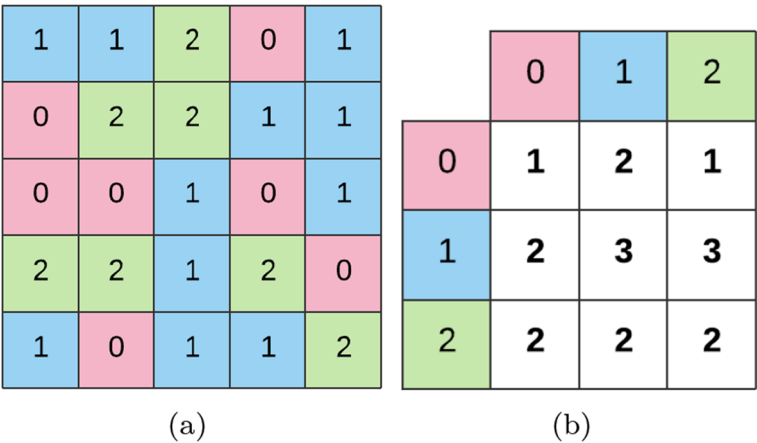

Fig. 4 **a** An example of a given matrix and **b** the computation of GLCM for the corresponding matrix depending on 0°

should be 1. After then, this process continues for every row and column numbers which constitute all the values in the GLCM.

2.1.4 Local phase quantization (LPQ)

LPQ firstly proposed for texture classification as a local texture descriptor in [34]. LPQ descriptor is based on quantized phase of discrete Fourier transform (DFT) computed locally in a window for every image patches. The algorithm uses the local phase information to characterize the underlying image texture. Mainly, the blurring effect produced by motion or imaging equipment can be handled by this algorithm.

2.1.5 Segmentation-based fractal texture analysis (SFTA)

SFTA is a texture based feature extraction algorithm proposed by Costa et al. for content based image retrieval task in [10]. SFTA consists of two parts: (i) decomposition of the gray-scale image to a set of binary images and (ii) calculation of fractal dimensions, mean gray-level, and size for each resulting binary image. In decomposition phase, a new algorithm called as two-threshold binary decomposition (TTBD) is proposed in [10]. TTBD takes the gray-scale image as input and returns multiple binary images. At the first part of TTBD, a set of thresholding values is calculated by using the Otsu thresholding method [35], which uses the distribution information of the gray level image. The number of images is determined by the number of thresholds. To segment the object accurately or to extract the region information successfully, the gray-level value of the specified area must be in the middle part of the histogram. So that, a two level thresholding algorithm can be applied to the image. Another point that should be realized is that an object can not be segmented successfully with a single threshold value. After applying the TTBD to the input image, the feature vector is constructed by calculating the fractal dimension of the size, mean gray level and boundaries of the input image.

2.1.6 Statistical based feature extraction algorithm

In this method, the statistical based discriminative features are tried to be extracted for mitosis detection purpose. In slides, coordinate information (top left, top right, bottom left, and bottom right) of the segmented cellular structures are stored for evaluation. Then, those mitotic and non-mitotic cellular structures are surrounded by a window to get image patches (as a region of interest) where features are extracted.

Blob analysis is a fundamental technique used in computer vision and image processing in a particular region. This particular region has certain properties that are considered constant or approximately constant. Therefore, it can be assumed that all pixels in a blob are similar. Basically, blob analysis is used to identify the connected components and extract statistical information about the selected connected components. Blob analysis facilitates to provide complementary information about regions. In this part of the study, blob analysis is applied to the image patches of cellular structures. There are also some noisy components which have a few number of pixels assumed as cellular structure in segmentation step. These noisy parts are eliminated to save only real cellular image patches for feature extraction. In Fig. 5, sample image representations of blob analysis for mitotic and non-mitotic cellular structures. The blob analysis is performed on the binary format of the given image patches. The yellow bounding box shows the border information of the image patch found by blob analysis.
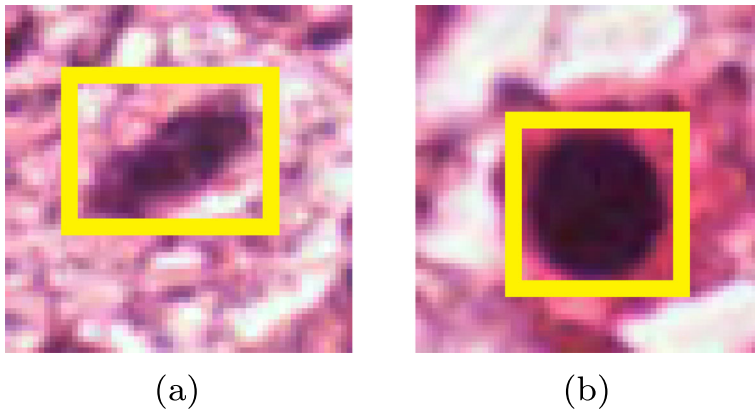
Fig. 5 Two image sample representation of blob analysis for **a** mitotic cell **b** non-mitotic cell

In blob analysis, width, height, minimum area, maximum area, axis lengths, orientation, perimeter and extent (i.e., dividing the areas of the blobs by the area of their bounding boxes) information can be extracted from image patches. Besides that, some other statistical information can also be extracted from image patches for obtaining discriminative features. Some statistics are employed by arranging image patches in a vector format as follows (where n describes the number of elements and x_i describes each element in the vector):

- *Mean*: It is the division of sum of all elements in the vector to the number of elements in the vector $\left(\mu = \left(\sum_{i=1}^{n} x_i\right) / n\right)$. In this step, the mean of each bands (red, green, blue) of an image patch is calculated and hereby, three features are extracted eventually.
- *Standard Deviation*: It is the measure of the dispersion/distribution of the vector from its mean $\left(\sigma = \sqrt{(1/n)\sum_{i=1}^{n} (x_i - \mu)^2}\right)$.
- *Skewness*: It is the measure of *non-symmetricity* of the data collected around the mean $\left(E (x - \mu)^3/\sigma^3\right)$, where E denotes the expected value. If the value of the skewness,

    – Skewness$> 0 \rightarrow$ it is called as right skewed distribution.
    – Skewness$< 0 \rightarrow$ it is called as left skewed distribution.
    – Skewness$= 0 \rightarrow$ it shows mean = median, the distribution is symmetrical around the mean.

- *Kurtosis*: It is the measure of the height and sharpness of the peak in data distribution $\left(E (x - \mu)^4/\sigma^4\right)$, where E denotes the expected value.

2.2 Deep learning based approach for feature extraction

Convolutional neural network (CNN) is a neural network based deep learning algorithm proposed by Le Cun & Bengian (1995) [29]. Deep learning is a machine learning algorithm that is proposed as an alternative method to the conventional classification and also feature extraction methods. The main advantage of deep learning is that it is adaptable to the given input raw data to extract the most distinguishable features. Convolutional layers, activation functions, pooling layers, fully connected layer and softmax layer (also called classification layer) are the layers that can be included in CNN architecture.

Convolutional layer: The image obtained from the input layer is convolved with generalized filters (like filter bank) size of $k \times k$ to extract the first order features such as edge or texture information of the image. The output of the convolution is called activation maps. The strong representation of the given image could be determined with activation maps. The output activation maps obtained from the first convolutional layer are the same with number of filters. The size of the activation maps differs depending on the padding size.

Activation function: Rectified Linear Unit (ReLU) performs a threshold operation for each element in the activation maps to pass to the next layer. If the element is less than a threshold value, then the elements' value is set to zero. The activated elements could be defined as the representative features of the image. The nonlinearity is introduced in this layer.

Pooling layer: The summary of the previous two layers (convolutional and ReLU function) are shown by this layer. The result maps obtained from convolutional layer and activated with ReLU function are then summarized by taking average or maximum of each neighborhood pixels in the specific size defined.

Fully-connected layer: This layer is the last and most important layer that takes the data from the flattening process and the learning process through the neural network.

Softmax layer: In the final layer of CNNs, the use of softmax layered units for multi-class classification is quite common.

In the feature extraction step, it is important to know that the cell structure undergoes a series of steps during the cell division process. During cell division, the chromosomes are pulled and move towards the spindle poles, the nucleus is almost destroyed, and the cells resemble a convex or concave structure. This makes it possible for a cell to be textually, statistically and morphologically different from a normal undivided cell. Therefore, statistical,
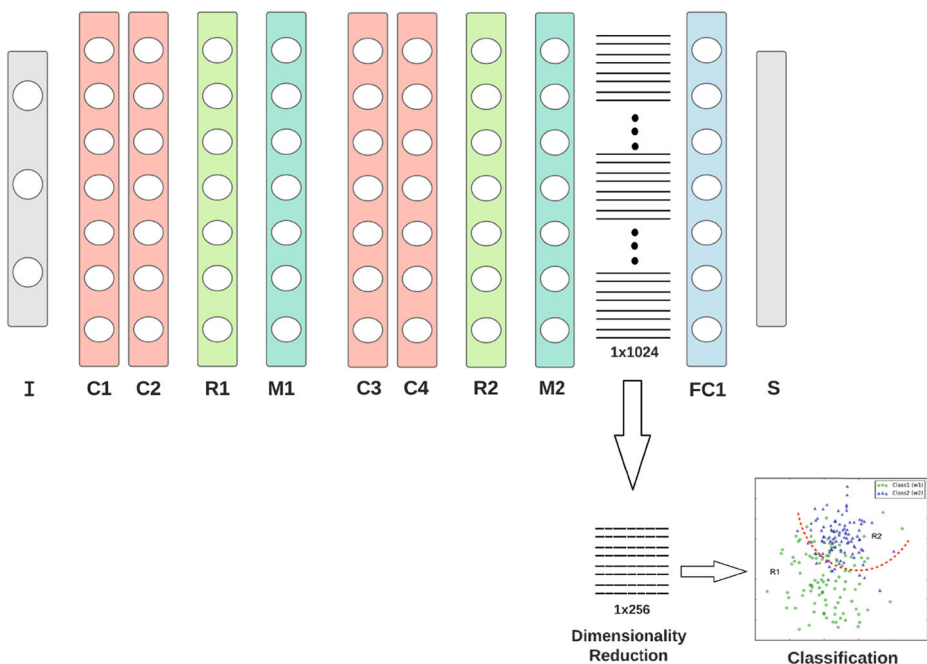

Fig. 6 The CNN architecture implemented in the proposed study

textual and shape-based analysis of mitosis detection is of great importance. In our study, all image patches of cellular structures obtained from histopathological slides are used in the feature extraction stage.

The network designed in this study is shown in Fig. 6. The symbols I, C, R, M, FC, D and S are the image input layer, convolutional layer, activation function, max-pooling layer, fully-connected layer and softmax classification layer. In the input layer, the image is converted by subtracting the mean of the image from the pixel values in the training set to reduce the overfitting. Low level features are extracted in the first convolution layers of CNN architectures and has crucial importance in image patches with small sizes. So, it is preferred to use 5×5 filter size in the first convolution layers since it contains more textural information than 3×3 filter size. To create feature maps, two convolution layers with kernel size of 5×5 with one stride and without padding are applied to the images in the dataset. The number of convolution filters at the first two layers are 64 and 128 respectively.

The third layer applied to each image has rectified linear units (ReLU), which perform a simple thresholding operation where an input value less than zero will be set to zero and an input value greater than zero will be activated for the next layers to be processed for further analysis. The activation function is followed by max-pooling, which divides the input image into rectangular regions with equal sizes, and outputs the maximum of each region. The max-pooling layer used after ReLU has a kernel size of 2×2. After max pooling layer, other two convolutional layers with a filter size of 3×3 are applied to each image with stride of 1 and without padding. This time the number of filters convoluted on the activation maps are set to 192 and 256, respectively. The convolutional layers are followed by a activation function and a max-pooling layer used after ReLU with a kernel size of 2×2. At this stage, fully connected layer and softmax layer are not used for further analysis. The extracted feature vectors obtained before the fully connected layer are classified with the RUSBoost algorithm for fair comparison with the other feature extraction algorithms. The dimensions of the feature vectors are reduced to 256 by calculating the eigenvalues considered to be the best representative. The sum of the first n eigenvalues is divided by the sum of all eigenvalues and the number that provides 95% is selected as the feature vector size.

3 The proposed CAD based mitosis detection approach

The aim of this study is to develop an effective and robust framework for detecting mitotic cells in histopathological images. The steps of the proposed method are described in this section and the explanatory flowchart is presented in Fig. 7.

The main purpose of our study is to detect mitosis from breast cancer histopathological images, which is one of the important criteria in breast cancer grading. In this study, histopathological images of breast cancer shared in the mitosis detection contest organized by the International Pattern Recognition Conference (ICPR) in 2014 are examined [41]. This contest in question actually consists of two parts: nuclear atypia score and mitosis detection. Histopathological images stained with Hematoxylin and Eosin (H&E) dyes were scanned by Aperio Scanscope XT ve Hamamatsu Nanozoomer 2.0-HT scanners. In the experiments, Aperio Scanscope XT histopathological images are used to detect mitosis at ×40 magnification. Some examples of images are shown in Fig. 8.

Information about the number of images in the dataset and the mitotic cells included in these images are given in Table 1. The dataset contains 749 mitotic cells in a total of 1200 high resolution histopathological images.
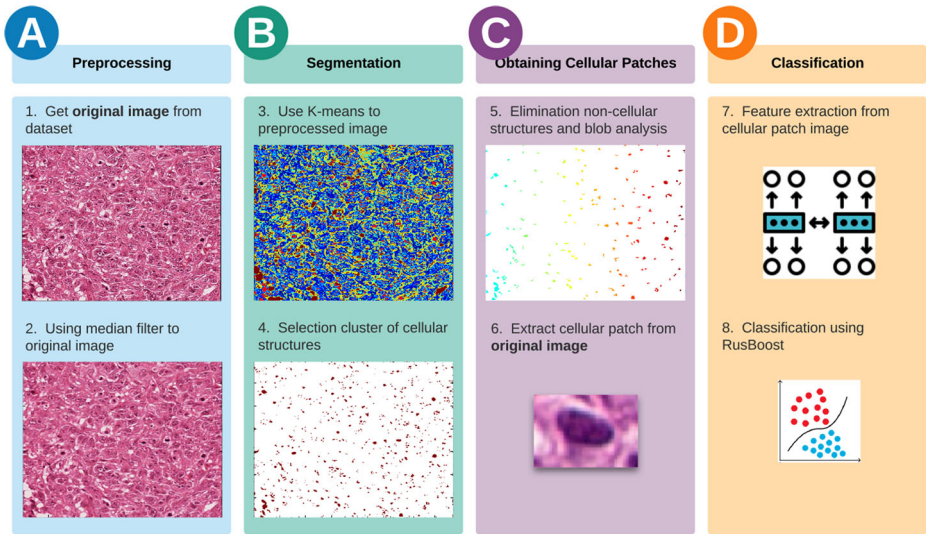
Fig. 7 The general structure of the pipeline followed for the framework

3.1 Preprocessing stage

Preprocessing is one of the most important stages of image processing, which is applied to improve certain features in images or remove undesired distortions. Preprocessing in histopathological images is an important step used to obtain more distinctive features. In particular, the boundaries of cellular structures should be preserved and properly determined during the preprocessing stage. In the preprocessing step of the proposed work, studies related to noise reduction by median filtering, pre-segmentation and proper selection of cellular structures are made.

Noise may occur when scanning high resolution histopathological images randomly. For better segmentation, noise should be removed as much as possible while preserving borders of cellular structures. Therefore, a median filter in size of 9×9 is applied to each band of

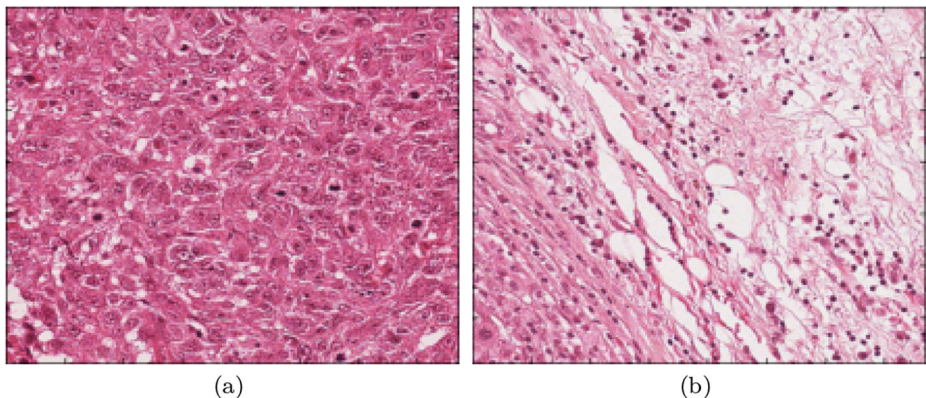(a)   (b)

Fig. 8 Example images selected from the dataset

Table 1 Information table for the number of images in each folder and the total number of mitotic cells in each folder for the unspecified patient

Folder	#Images	#Mitotic cells
A03	96	135
A04	128	264
A05	112	151
A07	64	39
A10	80	25
A11	128	20
A12	144	2
A14	160	33
A15	96	25
A17	80	34
A18	112	21
Total	**1200**	**749**

The total number of images and mitotic cells used in the data set are highlighted in bold

histopathological images. The Fig. 9 presents a zoomed-in sample cellular structure image patch and a filtered version of the same cell for visual assessment of the noise reduction.

After filtering to remove noise, cellular parts of the image should be revealed so that the nuclei are easily separated from background structures such as blood, stroma and adipose tissues.

3.2 Segmentation stage

For segmentation step, well-known k-means algorithm is applied on the filtered image patches. For the best value, after several experimental trials from 3 to 9 cluster centers (k),
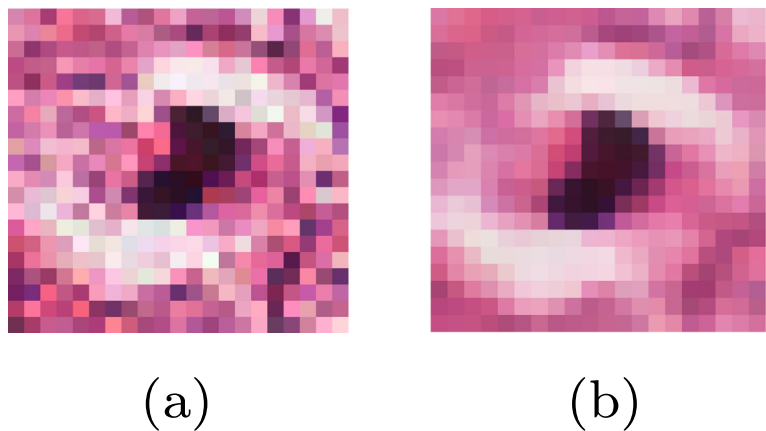

(a) (b)

Fig. 9 **a** A zoomed-in sample cell image patch taken from dataset and **b** median filtered version of the same cell
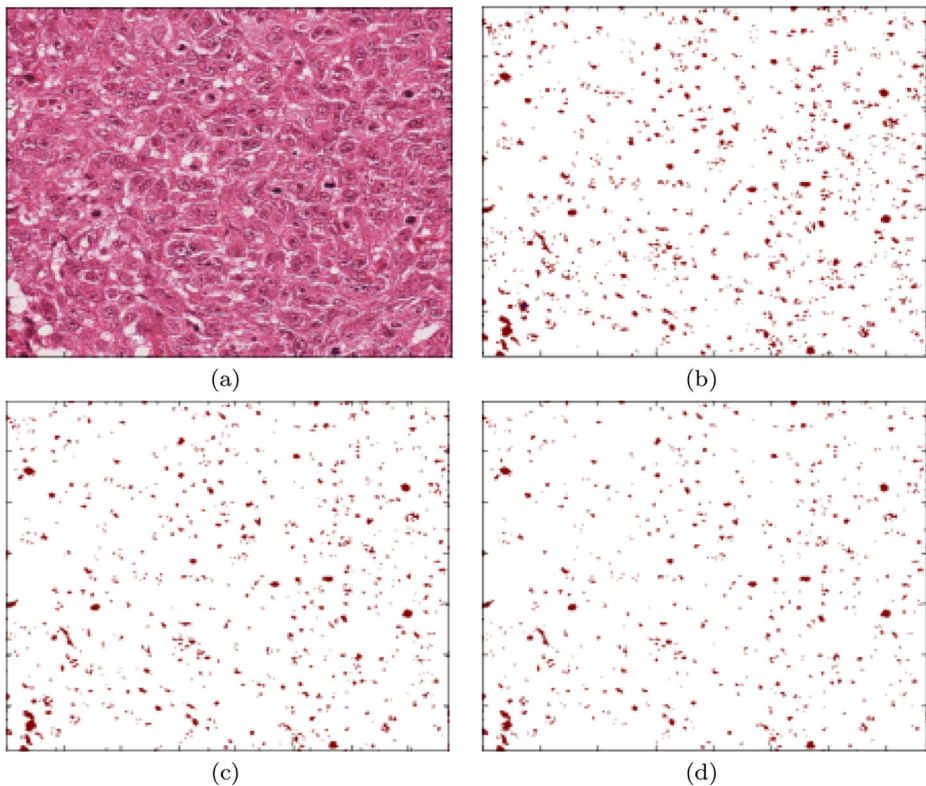
Fig. 10 **a** Original sample image and segmentation maps obtained by k-means algorithm for **b** $k = 7$, **c** $k = 8$, **d** $k = 9$ cluster centers

the k parameter is selected as 8 for segmentation. To select the best value for mitosis detection, after several experimental trials from 3 to 9 cluster centers (k), the parameter k is selected as 8 for segmentation..

In the example given in Fig. 10a, represents an original sample image to be clustered; b, c and d show the cellular structures in images obtained with 7, 8 and 9 cluster centers. When the k is chosen lower than eight clusters, the resulting cell nuclei borders are larger than the original borders. If the k parameter is chosen greater than eight clusters, obtained cell nuclei borders are narrower than the original borders.

The cellular structures have relatively low intensity values in histopathological images compared to other parts. Therefore, some small irrelevant particles which are segmented as cellular structure due to their low intensity values similar to the nuclei parts should be eliminated in the postprocessing of the segmentation. In Fig. 11, a zoomed segmented part around the cellular structure and extracted cellular part of interest are shown as an example.

3.3 Obtaining image patches of cellular structures

At this stage, it is proposed to form up different types of distinctive features to detect mitotic cells. Initially, the coordinate information (top left, top right, bottom left and bottom right) of the cellular structures segmented from the histopathological images in the dataset is stored
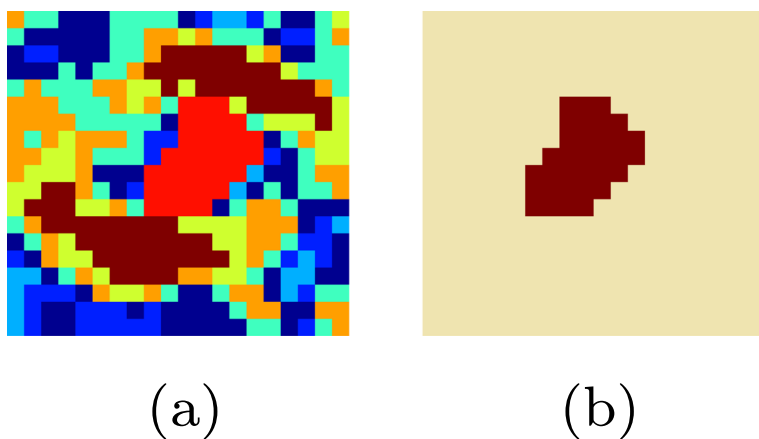
Fig. 11 **a** A zoomed segmented part around cellular structure and **b** extracted cellular part of interest

for evaluation. These stored mitotic and non-mitotic cellular structures are then framed by a window to create image patches (as a region of interest) from which the features are extracted.

3.4 The feature extraction stage

The detailed flowchart of the feature extraction step applied in this study is presented in Fig. 12. The cellular image patch dataset is created after pre-processing and segmentation stages which applied to the whole images obtained from the main dataset used in this study. All of cellular image patches are split into training and test data using a 5-fold cross validation. Each cellular image patch is given as input data to the shape, texture and statistical-based feature extraction algorithms and CNN based deep feature extraction model. In Fig. 12, the reason for adding "training" to the CNN algorithm in the feature extraction stage is that the CNN algorithm needs training data for deeper analysis. After the training of CNN model for each fold, the feature vectors are obtained both for the train and test image patches.

The CNN-based approach used in this study requires training, while other feature extraction algorithms do not require a training phase to obtain feature vectors. In this context, the
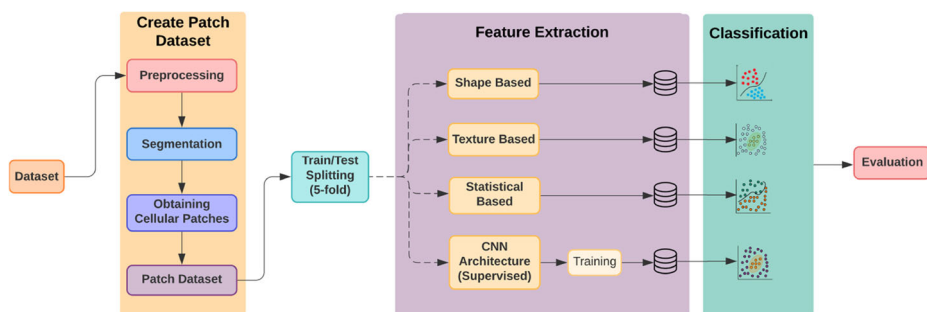

Fig. 12 Detailed flow of feature extraction stage of the proposed framework

proposed CNN approach can be considered as a fourth category in the feature extraction phase, except for shape, texture and statistical based methods. Feature vectors obtained to distinguish mitotic cells from non-mitotic cells are then subjected to a two-class classification in the classification stage. The results obtained from the different feature extraction methods are presented comparatively in Section 4.

3.5 Classification of imbalanced data via RUSBoost

The imbalanced data can be defined as data in which one or more classes have more instances than the others, i.e. the sample distribution is unbalanced. In this case, test samples of small classes are misclassified more often than prevalent classes. There are several studies in the literature to solve imbalanced data classification such as SMOTEboost (Synthetic Minority Over-sampling TEchnique) [3], DataBoost-IM approach [18], subset filtering based method [39] and RUSBoost (Random Under-Sampling Boosting) which is a boosting based algorithm proposed by C. Seiffert et al. to avoid the misclassification of imbalanced data [43].

Rusboost algorithm has been developed on SMOTEBoost algorithm which is another algorithm used for imbalanced data.

In addition to being simpler and faster than SMOTEboost, RusBoost provides better results in binary classifications, but cannot achieve similar performance in binary classifications in multiclass classifications [49]. Therefore, in this study, RUSBoost method is chosen as a simple and fast model to deal with imbalanced number of mitotic and non-mitotic cells. Random under-sampling basically removes samples arbitrarily from larger classes until it provides the desired balance between the classes. Naturally, removing the samples from the large class causes loss of information about that class. However, this handicap can then be addressed by boosting algorithm to produce new samples from existing ones.

Let each of $x_1, x_2, \ldots, x_m$ are samples of S dataset with m number of samples and $y_1, y_2, \ldots, y_m$ correspond to class labels of the related samples. In our study, y can take two values as mitotic and and non-mitotic. The processing steps of RUSBoost algorithm are given in Algorithm 1. In algoritm steps, the $WeakLearner$ represents a weak learner algorithm, T shows the number of iteration, h_t; represents the hypothesis used at t^{th} stage of $WeakLearner$'s training and $D_t(i)$ describes the weight used at t^{th} step for i^{th} sample.

Algorithm 1 RUSBoost algorithm.

---

1. For all i, $D_1(i) = 1/m$ is initialized.
2. Let t be the number of classifier ($t = 1, 2, \ldots, T$), each classifier is trained:

   (a) Using D'_t, a temporary dataset shown as S'_t is created with under-sampling.
   (b) S'_t and D'_t are given to $WeakLearner$.
   (c) $WeakLearner$ gives a weak hypothesis represented by h_t as a result.
   (d) ϵ_t error is calculated according to the S, original dataset, and D_t which represent the weight.
   (e) Using ϵ_t the weight update parameter, $\alpha = \epsilon_t/(1 - \epsilon_t)$ value is calculated.
   (f) The next t value, D_{t+1} weight distribution is created.
   (g) The D_{t+1} created weights are normalized.

3. After T iteration, the model returned as a result. The model is determined as weighted value of T weak learners.

In the first step of the algorithm, each sample is started with weights of $1/m$. In the second step, weak hypotheses are trained T times iteratively. Random under-sampling (RUS) removes majority class instances. For example, if the desired class ratio is 50 : 50, majority class instances are randomly removed until the numbers of majority and minority class instances are equal. The S'_t can be described as the result temporary dataset after RUS. The S'_t will have the new D'_t weight distribution. The S'_t and D'_t are given to the basic weak learner which creates the weak hypothesis. The error ϵ_t is calculated according to S training dataset and D_t weight distribution. The weight update parameter $\alpha = \epsilon_t/(1 - \epsilon_t)$ is calculated. Then, the D_{t+1} weight distribution is updated and normalized for the next iteration. After T iteration, the result is returned as the weighted vote of T weak hypotheses.

3.6 Classification stage

In this stage of the study, the feature vectors obtained from spatial feature extraction algorithms are utilized for classification. Approximately 180,000 non-mitotic and 749 mitotic cells were extracted from 1200 images cropped from ten whole slides. The accuracy of the proposed study is evaluated by using 5-fold cross-validation strategy. Classification is performed using the RUSBoost method, a robust and fast algorithm, especially for unbalanced two-class datasets.

4 Results

4.1 Dataset description

The dataset used in experiments is released at the International Conference on Pattern Recognition Conference (ICPR) with the MITOS-ATYPIA-14 contest [41]. The contest consists of two parts: Detection of mitosis, and evaluation of nuclear atypia score. The dataset images are breast cancer histopathological images which are stained with hematoxylin and eosin (H&E) dyes and scanned by Aperio Scanscope XT and Hamamatsu Nanozoomer 2.0-HT slide scanners. For this study, we mainly focus on mitotic cell detection in these high resolution histopathological images.

The training dataset is consist of frames at $\times 40$ magnification level extracted from ten slides of breast cancer samples. Each frame is an RGB image corresponding to a sample surface of approximately $379 \times 338 \ \mu m$ pixel size in TIFF format. The slides were scanned by Aperio scanner at size of 1539×1376 pixels with a resolution of 0.2455 μm/pixel. Mitotic cell annotations were provided by two senior pathologists and three junior pathologists of Pitie-Salpetriere Hospital and of Institut Curie, Paris France [41]. Histopathological images, magnified $\times 40$ and including mitotic formations, are evaluated by two different pathologists. The pathologists have annotated mitotic formations as true mitosis, probably a mitosis, or not a mitosis. In case of disagreement between the pathologists, a third pathologist identified the diagnosis and the cellular formation was marked as mitotic or non-mitotic by majority.

4.2 Evaluation of methods

The results of several textural, statistical and shape-based feature extraction methods are compared with the proposed CNN method. The number of true positives (TP), false positives (FP), false negatives (FN) and true negatives (TN) are obtained and precision, recall

and F-measure metrics are used to evaluate the mitosis detection of each method. These metrics used for comparison can be described as follows:

- TP: Mitotic cells correctly identified as mitotic.
- FP: Non-mitotic cells incorrectly identified as mitotic.
- FN: Mitotic people incorrectly identified as non-mitotic.
- TN: Non-mitosis cells correctly identified as non-mitotic.
- **Precision:** The fraction of retrieved instances that are relevant:

$$P = \frac{TP}{TP + FP} \tag{7}$$

- **Recall:** The fraction of relevant instances that are retrieved:

$$R = \frac{TP}{TP + FN} \tag{8}$$

- **F-Measure**= Harmonic mean of the precision and recall:

$$\text{F-Measure} = 2 \times \frac{P \times R}{P + R} \tag{9}$$

Cellular image patches obtained in segmentation stage are used as input to the each feature extraction method. The classification results are represented in Table 2. Each row in the table shows the applied feature extraction method. For each method, precision, recall and F-measure values are shown in the first, second, and third columns, respectively. According to the Table 2 obtained from the classification results, the proposed method has the highest precision and F-measure values and the second highest recall value after statistics-based method among all feature extraction methods. Although the SFTA algorithm is the most successful among conventional feature extraction methods (except CNN based proposed method) in precision, approximately 8.55% of non-mitotic cells are misclassified after resampling with RUSBoost algorithm. The proposed CNN based algorithm produces the most accurate result in the classification of both mitotic and non-mitotic cells. The confusion matrices of all seven methods are given in Table 3 for comparison purposes.

The accuracy of the proposed study is evaluated by using 5-fold cross-validation strategy. The CNN architecture is built as described in Section 2.2 and the network is trained by stochastic gradient descent (SGD) with learning rate of 0.01, momentum value of 0.6 and the epoch size of 100.

Table 2 Precision, recall, and F-measure values of each feature extraction algorithm

	Precision	Recall	F-Measure
CLBP	0.857797	0.746439	0.798253
HOG	0.843037	0.726496	0.780439
Haralick	0.807412	0.720798	0.761650
LPQ	0.818678	0.695157	0.751878
SFTA	0.898879	0.760684	0.824028
Statistics	0.875803	0.806268	0.839598
CNN-based approach	0.967821	0.794203	0.869701

Table 3 Confusion matrices of RUSBoost classifier for each feature extraction algorithms (NM: Non-Mitotic Cells, M: Mitotic Cells)

			Predicted (%)	
			NM	M
Actual(%)	CLBP	NM	87.6258	12.3742
		M	25.3561	74.6439
	HOG	NM	86.4735	13.5265
		M	27.3504	72.6496
	Haralick	NM	82.8072	17.1928
		M	27.9202	72.0798
	LPQ	NM	84.6036	15.3964
		M	30.4843	69.5157
	SFTA	NM	91.4426	8.5574
		M	23.9316	76.0684
	Statistics	NM	88.5663	11.4337
		M	19.3732	80.6268
	CNN-based approach	NM	96.7821	3.2179
		M	20.5797	79.4203
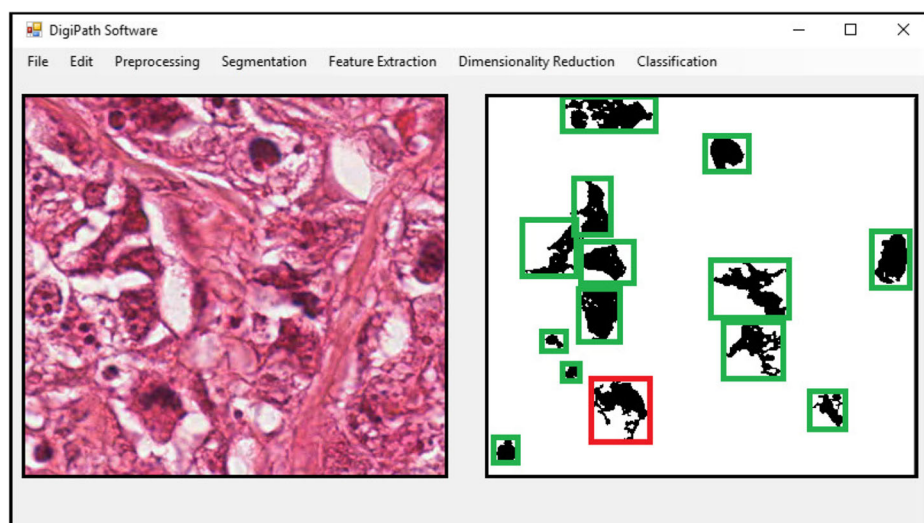
Fig. 13 A sample screenshot from DigiPath computer aided diagnosis software. Thanks to the developed program, different preprocessing, segmentation, feature extraction, dimensionality reduction and classification methods can be used in the detection of mitotic cells in histopathological images

5 Application software

In order to facilitate the workload of pathologists working on histopathology data, a software called DigiPath has been developed with a graphical user interface containing the methods mentioned in the Section 2 section. The utility software uses python libraries as backend and C# programming language as frontend. An example screenshoot of DigiPath software is presented in Fig. 13. The "File" menu specified in the menustrip of the GUI can be used to perform simple operations such as opening a single image or list of images in a folder, "saving" or "save as" file, and closing the program. In addition, menus have been created in the menustrip for basic image processing and pattern recognition steps, including pre-processing, segmentation, feature extraction, dimensionality reduction and classification. Several submenus, which indicate the name of the algorithm under the relevant menu, can be arranged according to the required parameters for each selected algorithm.

6 Conclusions

Morphological changes of cellular structures cause significant and distinctive differences between mitotic and non-mitotic cells in histopathological images. In the mitotic stage, the nuclear membrane disappears and chromatin strands move towards the center position of the cell. However, non-mitotic cells are mostly elliptical structures and also have elliptical nuclei. These morphological changes in mitotic cells also make a difference on the density values of the related pixels. For these reasons, statistical, shape based and textural descriptors can be utilized to classify mitotic and non-mitotic cells. In addition to conventional algorithms, deep learning based algorithms are also used for feature extraction in recent years. In this study, a CNN based deep learning is employed in a comparative way with the handcrafted methods and the results are presented in the experimental studies. The implemented methods are tested on mitosis detection in the breast cancer histological image dataset provided for the International Pattern Recognition Conference (ICPR) 2014 contest. For the given dataset, approximately 180,000 non-mitotic and 748 mitotic cells are extracted from 1200 images cropped from 10 histopathological whole slides. The proposed deep learning based approach achieved 96.78% precision, 79.42% recall and 86.97% F-measure values. According to the results, the proposed method has the highest precision and F-measure values; the second highest recall value after statistical based method among all feature extraction methods.

Within the scope of the study, an application software called DigiPath has been developed with a graphical user interface containing the methods discussed in this article. In this way, it is aimed to facilitate the workload and analyze the test images more easily for the detection of mitosis in histopathological images.

7 Discussion and future work

In the proposed system, it was focused on the detection of mitosis in high resolution histopathological images. Since morphological changes in mitotic cells make a difference on the textural intensity values of the related pixels, spatial examination of the tissue helps to achieve distinctive features. For this reason, GLCM, LBP and SFTA algorithms are used as prominent spatial/textural feature extraction algorithms. In addition to these methods, statistical features such as mean, standard deviation, skewness and kurtosis are employed as

statistical based feature extraction approach to obtain the characteristics of mitotic cells. In addition to these statistical features, the extent, concavity and convexity based shape information features are appended to the feature vector to determine the shape changes of mitotic cells using the blob analysis approach. The classification results show that deep learning-based feature extraction is superior to others in determining mitotic structures. The main advantage of deep learning is that it is adaptable to the input raw data to obtain the most distinctive features. However, feature extraction algorithms, other than deep learning, are problem-specific algorithms. One reason that deep learning has been on the rise in recent years is the developments in graphics processing units (GPU) technology. In general, the deep learning training phase takes a lot of time to learn data, but using GPUs makes this process faster than CPUs. In the proposed study, since the image patches of cellular structures have small sizes of of 32×32 pixels, two convolutional layers are used one after another. Applying only a single convolutional layer may not be sufficient to extract distinctive features because the use of the maximum pooling layer will reduce the size of the image in the next layer. Instead, more discriminatory features are extracted by using two successive convolutional layers, and then the size of the activation maps is reduced.

Many classification algorithms are not robust in classifying imbalanced data such as mitosis detection dataset containing 180,000 non-mitotic cells and 749 mitotic cells. The precision value may be high but the recall value is so crucial especially in histopathological images. As a solution to this problem, RUSBoost basically removes samples arbitrarily from larger classes until they achieve the desired balance between classes. Naturally, removing the samples from the large class causes loss of information about this class. However, this handicap can be handled later by boosting the algorithm to produce new samples from the existing ones. In future studies, we plan to concentrate on the robustness of deep learning algorithms in imbalanced datasets.

References

1. Bloom H, Richardson W (1957) Histological grading and prognosis in breast cancer: A study of 1409 cases of which 359 have been followed for 15 years. Br J Cancer 11(3):359–377
2. Chan TH, Jia K, Gao S, Lu J, Zeng Z, Ma Y (2015) Pcanet: A simple deep learning baseline for image classification? IEEE Trans Image Process 24(12):5017–5032
3. Chawla NV, Lazarevic A, Hall LO, Bowyer KW (2003) Smoteboost: Improving prediction of the minority class in boosting. In: European conference on principles of data mining and knowledge discovery in databases, PKDD'03. Springer, pp. 107–119
4. Chen Y, Lin Z, Zhao X, Wang G, Gu Y (2014) Deep learning-based classification of hyperspectral data. IEEE J Sel Top Appl Earth Obs Remote Sens 7(6):2094–2107
5. Chen LC, Papandreou G, Kokkinos I, Murphy K, Yuille AL (2016) Deeplab: Semantic image segmentation with deep convolutional nets, atrous convolution, and fully connected crfs. arXiv:1606.00915
6. Cheng JZ, Ni D, Chou YH, Qin J, Tiu CM, Chang YC, Huang CS, Shen D, Chen CM (2016) Computer-aided diagnosis with deep learning architecture: applications to breast lesions in us images and pulmonary nodules in ct scans. Sci Rep 6:1–13
7. Cheng J, Veronika M, Rajapakse JC (2010) Identifying cells in histopathological images. In: Recognizing patterns in signals, speech, images and videos. Springer, pp. 244–252
8. Ciresan DC, Giusti A, Gambardella LM, Schmidhuber J (2013) Mitosis detection in breast cancer histology images with deep neural networks. In: International conference on medical image computing and computer-assisted intervention, MICCAI'13. Springer, pp. 411–418

9. Collaborative Group on Hormonal Factors in Breast Cancer et al (2002) Breast cancer and breastfeeding: collaborative reanalysis of individual data from 47 epidemiological studies in 30 countries, including 50 302 women with breast cancer and 96 973 women without the disease. Lancet 360(9328):187–195

10. Costa AF, Humpire-Mamani G, Traina AJM (2012) An efficient algorithm for fractal analysis of textures. In: 25th IEEE SIBGRAPI conference on graphics, patterns and images, pp 39–46

11. Dalal N, Triggs B (2005) Histograms of oriented gradients for human detection. In: IEEE computer society conference on computer vision and pattern recognition, CVPR'05, vol. 1, pp 886–893

12. Dalle JR, Leow WK, Racoceanu D, Tutac AE, Putti TC (2008) Automatic breast cancer grading of histopathological images. In: 30th IEEE annual international conference of the engineering in medicine and biology society, EMBC'08, pp 3052–3055

13. De Angelis R, Sant M, Coleman MP, Francisci S, Baili P, Pierannunzio D, Trama A, Visser O, Brenner H, Ardanaz E et al (2014) Cancer survival in europe 1999–2007 by country and age: results of eurocare-5—a population-based study. Lancet Oncol 15(1):23–34

14. Dundar MM, Badve S, Bilgin G, Raykar V, Jain R, Sertel O, Gurcan MN (2011) Computerized classification of intraductal breast lesions using histopathological images. IEEE Trans Biomed Eng 58(7):1977–1984

15. Elston CW, Ellis IO (1991) Pathological prognostic factors in breast cancer. i. the value of histological grade in breast cancer: experience from a large study with long-term follow-up. Histopathology 19(5):403–410

16. Felzenszwalb PF, Girshick R, McAllester D, Ramanan D (2010) Object detection with discriminatively trained part-based models. IEEE Trans Pattern Anal Mach Intell 32(9):1627–1645

17. Gençtav A., Aksoy S, Önder S (2012) Unsupervised segmentation and classification of cervical cell images. Pattern Recognit 45(12):4151–4168

18. Guo H, Viktor HL (2004) Learning from imbalanced data sets with boosting and data generation: the databoost-im approach. ACM SIGKDD Explor Newsl 6(1):30–39

19. Gurcan MN, Pan T, Shimada H, Saltz J (2006) Image analysis for neuroblastoma classification: Segmentation of cell nuclei. In: 28th Annual international conference of the IEEE engineering in medicine and biology society, EMBC'06, pp 4844–4847

20. Hafiane A, Bunyak F, Palaniappan K (2008) Clustering initiated multiphase active contours and robust separation of nuclei groups for tissue segmentation. In: 19th International conference on pattern recognition, ICPR'08, pp 1–4

21. Hagwood C, Bernal J, Halter M, Elliott J (2012) Evaluation of segmentation algorithms on cell populations using cdf curves. IEEE Trans Med Imaging 31(2):380–390

22. Haralick RM, Shanmugam K (1973) Textural features for image classification. IEEE Trans Sys Man Cybern 6:610–621

23. He K, Zhang X, Ren S, Sun J (2016) Deep residual learning for image recognition. In: Proceedings of the IEEE conference on computer vision and pattern recognition, pp 770–778

24. Irshad H, Jalali S, Roux L, Racoceanu D, Hwee LJ, Le Naour G, Capron F (2013) Automated mitosis detection using texture, SIFT features and HMAX biologically inspired approach. J Pathol Inform, vol 4 (Suppl)

25. Irshad H, Roux L, Racoceanu D (2013) Multi-channels statistical and morphological features based mitosis detection in breast cancer histopathology. In: 35th IEEE annual international conference of the engineering in medicine and biology society, EMBC'13, pp 6091–6094

26. Khan AM, El-Daly H, Rajpoot NM (2012) A gamma-gaussian mixture model for detection of mitotic cells in breast cancer histopathology images. In: 21st IEEE international conference on pattern recognition, ICPR'12, pp 149–152

27. Krawczyk B, Jelen L, Krzyzak A, Fevens T (2012) Oversampling methods for classification of imbalanced breast cancer malignancy data. In: Comput. Vis. and Graph., Springer, pp 483–490

28. Krawczyk B, Jelen L, Krzyzak A, Fevens T (2014) One-class classification decomposition for imbalanced classification of breast cancer malignancy data. In: Artificial intelligence and soft computing, pp 539–550

29. LeCun Y, Bengio Y et al (1995) Convolutional networks for images, speech, and time series. Handb Brain Theory Neural Netw 3361(10):1995

30. Litjens G, Sánchez CI, Timofeeva N, Hermsen M, Nagtegaal I, Kovacs I, Hulsbergen-Van De Kaa C, Bult P, Van Ginneken B, Van Der Laak J (2016) Deep learning as a tool for increased accuracy and efficiency of histopathological diagnosis. Sci Rep 6:26286

31. Liu AA, Li K, Kanade T (2010) Mitosis sequence detection using hidden conditional random fields. In: IEEE international symposium on biomedical imaging: From Nano to Macro, ISBI'10, pp 580–583

32. M Naqi S, Sharif M (2017) Recent developments in computer aided diagnosis for lung nodule detection from ct images: A review. Curr Med Imaging Rev 13(1):3–19

33. Ojala T, Pietikainen M, Maenpaa T (2002) Multiresolution gray-scale and rotation invariant texture classification with local binary patterns. IEEE Trans Pattern Anal Mach Intell 24(7):971–987
34. Ojansivu V, Heikkila J (2008) Blur insensitive texture classification using local phase quantization. In: Image and signal Process. Springer, pp. 236–243
35. Otsu N (1979) A threshold selection method from gray-level histograms. IEEE Trans Syst Man Cybern 9(1):62–66
36. Ouyang W, Wang X (2013) Joint deep learning for pedestrian detection. In: Proceedings of the IEEE international conference on computer vision, ICCV'13, ppp 2056–2063
37. Paul A, Dey A, Mukherjee DP, Sivaswamy J, Tourani V (2015) Regenerative random forest with automatic feature selection to detect mitosis in histopathological breast cancer images. In: International conference on medical image computing and computer-assisted intervention MICCAI'15, Springer, pp 94–102
38. Porter P (2008) Westernizing women's risks? breast cancer in lower-income countries. N Engl J Med 358(3):213–216
39. Rao KN, Rao TV, Laksmi R (2012) A novel class imbalance learning method using subset filtering. Int J Sci Eng Res 3:95–103
40. Ren S, He K, Girshick R, Sun J (2015) Faster r-cnn: Towards real-time object detection with region proposal networks. In: Advances in neural information processing systems, pp 91–99
41. Roux L, Racoceanu D, Capron F, Calvo J, Attieh E, Le Naour G, Gloaguen A (2012) Mitos & Atypia detection of mitosis and evaluation of nuclear atypia score in breast cancer histological images. http://mitos-atypia-14.grand-challenge.org. Online; Accessed 2018-01-15
42. Rybski PE, Huber D, Morris DD, Hoffman R (2010) Visual classification of coarse vehicle orientation using histogram of oriented gradients features. In: IEEE intelligent vehicles symposium, IV'10, pp 921–928
43. Seiffert C, Khoshgoftaar TM, Van Hulse J, Napolitano A (2010) Rusboost: A hybrid approach to alleviating class imbalance. IEEE Trans Syst Man Cybern A Sys Hum 40(1):185–197
44. Sertel O, Catalyurek UV, Shimada H, Guican M (2009) Computer-aided prognosis of neuroblastoma: Detection of mitosis and karyorrhexis cells in digitized histological images. In: 31st IEEE annual international conference of the engineering in medicine and biology society, EMBC'09, pp 1433–1436
45. Siegel RL, Miller KD, Jemal A (2016) Cancer statistics, 2016. CA: A Cancer J Clin 66(1):7–30
46. Sommer C, Fiaschi L, Hamprecht F, Gerlich DW et al (2012) Learning-based mitotic cell detection in histopathological images. In: 21st IEEE international conference on pattern recognition, ICPR'12, pp 2306–2309
47. Suzani A, Rasoulian A, Seitel A, Fels S, Rohling RN, Abolmaesumi P (2015) Deep learning for automatic localization, identification, and segmentation of vertebral bodies in volumetric mr images. In: SPIE medical imaging, International society for optics and photonics, pp 941514–941514
48. Todoroki Y, Han XH, Iwamoto Y, Lin L, Hu H, Chen Y (2017) Detection of liver tumor candidates from ct images using deep convolutional neural networks. In: International conference on innovation in medicine and healthcare, Springer, pp 140–145
49. Van Hulse J, Khoshgoftaar TM, Napolitano A (2007) Experimental perspectives on learning from imbalanced data. In: Proceedings of the 24th international conference on machine learning, pp 935–942
50. Wan S, Huang X, Lee HC, Fujimoto JG, Zhou C (2015) Spoke-lbp and ring-lbp: New texture features for tissue classification. In: IEEE 12th international symposium on biomedical imaging, ISBI'15, pp 195–199
51. Wan T, Liu X, Chen J, Qin Z (2014) Wavelet-based statistical features for distinguishing mitotic and non-mitotic cells in breast cancer histopathology. In: IEEE international conference on image processing, ICIP'14, pp 2290–2294
52. Zhan T, Chen Y, Hong X, Lu Z, Chen Y (2017) Brain tumor segmentation using deep belief networks and pathological knowledge. CNS Neurol Disord Drug Targets (Formerly Curr Drug Targets-CNS Neurol Disorde) 16(2):129–136

Affiliations

I. Onur Sigirci[1] · Abdulkadir Albayrak[2] · Gokhan Bilgin[3]

1   Department of Computer Engineering, YTU, 34220 Istanbul, Turkey and SIMPLAB in YTU, 34220 Istanbul, Turkey

2   Department of Computer Engineering, Dicle University, 21280 Diyarbakir, Turkey and SIMPLAB in YTU, 34220 Istanbul, Turkey

3   Department of Computer Engineering, Yildiz Technical University (YTU), 34220 Istanbul, Turkey and Signal and Image Processing Lab. (SIMPLAB) in YTU, 34220 Istanbul, Turkey